

Binding Mechanism and Surface-Enhanced Raman Scattering of the Antimicrobial Sulfathiazole on Gold Nanoparticles

Tran Ni Kha, Nguyen Thanh Si, Van Man Tran, Khuong Quoc Vo, Minh Tho Nguyen,* and Pham Vu Nhat*



Cite This: *ACS Omega* 2023, 8, 43442–43453



Read Online

ACCESS |



Metrics & More

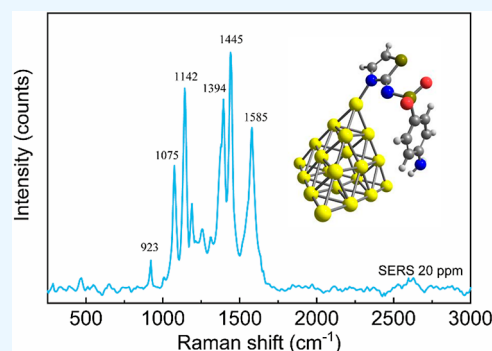


Article Recommendations



Supporting Information

ABSTRACT: A combined study using the surface-enhanced Raman scattering (SERS) technique and quantum chemical calculations was carried out to elucidate the adsorption behavior of sulfathiazole, an antibiotic drug, on gold nanoparticles. The tetrahedral Au₂₀ cluster was used as a simple model to mimic a nanostructured gold surface. Computations using density functional theory with the PBE functional were performed in both the gas phase and aqueous medium using a continuum model. The drug is found to bind to the Au metals via the nitrogen of the thiazole ring. The interaction is also partially stabilized by the ring-surface π coupling rather than a sideways adsorption as previously proposed. In an aqueous solution, the drug molecule mainly exists as a deprotonated form, which gives rise to a much greater affinity toward Au nanoparticles as compared to the neutral forms. The drug adsorption further induces a significant alteration on the energy gap of the gold cluster Au_n, which could result in an electrical noise. Notable SERS signals below 1600 cm⁻¹, which result from a coupling of several vibrations including the ring breathing, C–C stretching, and N–H bending, could be employed for both qualitative and quantitative detection and assessment of sulfathiazole at trace concentrations.



1. INTRODUCTION

Sulfathiazole, formally named as 4-amino-*N*-2-thiazolyl-benzenesulfonamide (STZ, [Figure 1](#)), is a powerful primary bioactive agent that is widely used as a short-acting sulfonamide drug for the prevention and cure of bacterial infections.¹ In practice, the drug is especially preferred for treatments of the respiratory

tract and digestive system, skin, and urinary tract infections in both humans and animal therapy.² Moreover, as a member of the sulfa drug family, the compound has also been utilized to improve the feed conversion rate and promote animal growth.³ As a diuretic, antiglaucoma or antiepileptic, STZ is often used under the forms of metal complexes because the complexes exert a much better activity than that of the isolated ligand.⁴ However, the abuse and excessive drug residues may cause some unexpected effects including the resistance of several bacterial species.⁵ In this context, the development of simple but powerful techniques for the selective and rapid detection of such drugs is of great pharmaceutical importance.

In recent decades, nanostructured materials have become more and more widely used as an efficient approach for the diagnosis and treatment of diseases.^{6–9} Of the popular inorganic nanostructures such as oxides and noble metals,^{10,11} those consisting of gold (Au) particles have peaked special attention as they exhibit unique properties and distinct advantages.¹² Indeed, gold nanoparticles (AuNPs) are highly compatible to a plenty of bimolecular systems and in particular

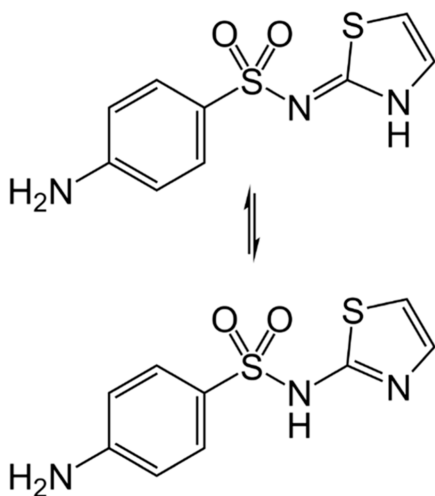


Figure 1. Two dominant tautomeric forms, imino (above) and amino (below), of sulfathiazole (STZ).

Received: March 4, 2023

Accepted: September 18, 2023

Published: November 7, 2023



they are much less toxic to human as compared to many other metals.¹³ Such tiny particles also pose a striking thermodynamic stability and are eager to be functionalized by a variety of biomolecules including drugs, amino acids, proteins, and various targeting ligands.¹⁴ They are also expected to enhance optical properties, surface plasmon resonance phenomenon, distinctive surface and macroscopic quantum tunneling effects,¹⁵ and are able to penetrate through the cell membrane without creating pores on the cell membrane.¹⁶ As a consequence, AuNPs turn out to be one of the most efficient ingredients for several biomedical uses such as biosensing, molecular imaging, drug delivery, etc.^{17–19}

Several theoretical and experimental approaches have been performed to validate the structures, energetics, along with electronic and spectroscopic features of STZ and its derivatives as well.^{1,20} Their adsorption behaviors on Cu, Ag, and Au nanostructured surfaces have also been examined by the surface-enhanced Raman scattering (SERS) technique.^{21,22} Accordingly, it was demonstrated that the SERS method could be a highly practical analytical technique for the detection of trace amounts of STZ residues in swine urine.²² In particular, the experimental SERS spectrum of STZ in Au colloid recorded by Ratkaj and Miljanic²¹ showed two dominant bands centered at 1590 and 1080 cm^{-1} that were assumed to arise from the phenyl ring stretching and C–H bending modes, respectively. These authors in addition proposed a sideways adsorption of STZ on the Au plate, with the phenyl moiety lying perpendicular and the thiazole ring being parallel toward the metal surfaces. Overall, the interaction of STZ with Au metals is mainly dominated by a Au–N bond and partially stabilized by the Au...H–C coupling. Nonetheless, it remains ambiguous whether either the amide nitrogen or the thiazole nitrogen is mostly responsible for the strong interacting Au–N bond.

Irrespective of several studies devoted to the interactions of STZ with AuNPs,^{21,22} there still exist many intrinsic limitations associated with these efforts. Indeed, the binding modes, energetic properties, and the SERS chemical enhancement of such sulfa drugs by Au nanostructured surfaces remain not fully elucidated. In this context, we set out to examine in the present study, as an attempt to reveal the adsorption behaviors of STZ molecules on the Au nanosurfaces, using both experimental and computational methods. More especially, in an effort to provide us with more thorough insights into the nature of interactions between these molecules and gold nanoparticles, a SERS experiment is carried out. Both normal Raman features and the SERS phenomenon of STZ molecules adsorbed on gold nanoparticles are experimentally recorded and thoroughly interpreted with the aid of quantum chemical approaches. Accordingly, three small gold clusters Au_n, with $n = 6, 8, 20$ are employed as simple model reactants representing the gold nanostructured surfaces. As a result of the quantum-size effects of metallic nanostructures, such studies are challenging but important, as some abnormal features and properties can be attained.

2. EXPERIMENTAL SECTION

2.1. Preparation of the Seed Colloidal Solution. The colloidal seed samples for prepared AuNPs are synthesized via the seed-mediated approach previously described^{23,24} with some changeovers. Typically, 10 μL of 25.0 M TSC aqueous solution is added into the 15 mL aqueous solution of 0.25 mM HAuCl₄, followed by magnetic stirring at the rate of 600 rpm

for 20 min. After the mixture was stirred, a 50 μL volume of 0.1 M NaBH₄ aqueous solution, freshly prepared and kept at 4 °C, is dropped into the above reaction mixture. Magnetic stirring is continuously maintained throughout the preparation process at 600 rpm. The colloidal solution containing gold nanoparticles can easily be prepared and noticed from the change of color from yellow to red purple for 30 s after pipetting the NaBH₄ aqueous solution. All seed samples do not go through stirring and are stored in the darkness for 3 h at 27 °C for further use in the synthetic process of AuNPs.

2.2. Preparation Process of Small Size Gold Nanoparticles. Gold nanoparticles with a small size, approximately 15 nm, are prepared by a typical process. The synthesis reaction is carried out with citric acid (CA) as a reducing agent, a seed colloid, and growth solutions. Typically, 10 mL of Millipore water is mixed with 100 μL of 25 mM HAuCl₄ and 10 μL of the seed solution into a 20 mL vial. The reaction mixture is stirred at 500 rpm at room temperature for 10 min. Then, a 22 μL volume of 1.0% (v/v) CA is dropped into the above reaction mixture. Subsequently, 100 μL of a 0.03 M hydroquinone solution is dropped slowly into the mixture to form the small-size AuNPs. The mixture color changes apparently from transparent yellow to red for 5 min, indicating the formation of small-size AuNPs.

2.3. SERS Characterization. In this study, sulfathiazole for Raman and SERS investigations with a purity $\geq 98\%$ (HPLC, analytical grade) is obtained from Shanghai Yuanye Biotechnology Co., Ltd. (Shanghai, China). The improvement of SERS signal intensity can be achieved from the intersection space between two small silver nanoparticles or on the surface of single particles. Sulfathiazole could be deposited onto the AuNP substrates through either Au–N or Au–S interaction with the presence of these atoms in the heterocyclic aromatic ring in the molecular formula of sulfa-thiazole. For evaluating the SERS enhancement activity of AuNPs for the detection of sulfathiazole, three comparison experiments of SERS studying are conducted, including a solid substance, 100 ppm solution without using small-size AuNPs, and the sample of 20 ppm sulfa-thiazole solution investigated with the AuNP substrates.

As shown in Figure 2, the AuNP substrate exhibits excellent intensity of Raman peaks positioned at 1142, 1394, 1445, and 1585 cm^{-1} . A slight shift of the peak position is observed in the spectra of solution samples compared to that of the solid sulfathiazole (Figure 2a–c). The sharp peak located at 1583 cm^{-1} is attributed to the stretching vibration of the benzene ring.^{25,26} Moreover, the peak of 1142 cm^{-1} is attributed to the SO₂ group in the molecular structure of sulfa-thiazole.^{27,28} The peak centered at 1585 cm^{-1} is selected to detect sulfathiazole using the small-sized AuNPs substrate. Besides, the peak located at 732 cm^{-1} only appears in the spectrum of sulfathiazole solid substances (Figure 2b). This peak disappears in the solution samples investigated with the AuNP substrate.

3. COMPUTATIONAL METHODS

Quantum chemical calculations for both equilibrium structures and energetic and spectroscopic properties are carried out by means of density functional theory (DFT) approaches using the Gaussian 16 package.²⁹ Local minima of all species considered are located with the Perdew–Burke–Ernzerhof (PBE) functional³⁰ inclusive of a mixed basis set, i.e., the effective core potential (ECP) cc-pVTZ-PP³¹ for Au atoms and the cc-pVTZ for STZ. Harmonic vibrational frequencies

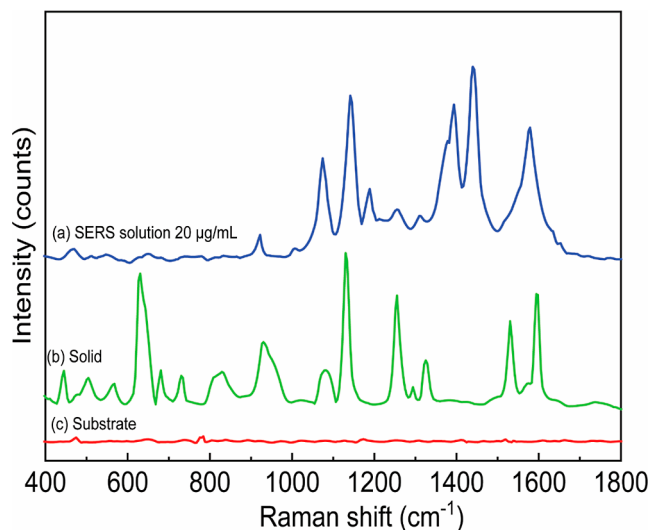


Figure 2. Experimental Raman spectrum of the Au nanosubstrate (curve a), SERS spectrum of STZ aqueous solution investigated with the AuNPs substrate (curve b), and Raman spectrum of sulfathiazole solid substances (curve c). Measurements are operated at 532 nm of an excitation source and 50 mW laser power selected at 100% with exposure times of 15 s and accumulation times of 2.

are then computed at the same level to characterize the stationary points as true local minima and to evaluate the zero-point energy (ZPE) corrections. The integral equation formalism-polarizable continuum model (IEF-PCM),³² a continuum model, is employed to simulate the solvent effects in aqueous solution.

The binding energy (E_b) is computed as the energy difference between Au_n -STZ complexes and segregated species using the following eq 1

$$E_b = (E_{Au_n} + E_{STZ}) - E_{Au_n-STZ} \quad (1)$$

where E_{Au_n-STZ} is the energy of the E_{Au_n-STZ} complexes, while E_{Au_n} and E_{STZ} are the energies of Au_n and STZ moieties, respectively. This parameter can be used to estimate the strength of the interactions, i.e., a more positive E_b corresponding to a stronger affinity of STZ molecules with Au metals.

The changes of enthalpy (ΔH°) and Gibbs free energy (ΔG°) during the interaction are evaluated following eqs 2 and 3

$$\Delta H = (E + H_{\text{corr}})_{Au_n-STZ} - [(E + H_{\text{corr}})_{Au_n} + (E + H_{\text{corr}})_{STZ}] \quad (2)$$

$$\Delta G = (E + G_{\text{corr}})_{Au_n-STZ} - [(E + G_{\text{corr}})_{Au_n} + (E + G_{\text{corr}})_{STZ}] \quad (3)$$

where $(E + H_{\text{corr}})$ is the sum of electronic energy and thermal enthalpies, $(E + G_{\text{corr}})$ the sum of electronic and thermal free energies.³³ The subscript “corr” in eqs 2 and 3 stands for the thermal correction to enthalpy or Gibbs free energy.

Energy levels of frontier orbitals, i.e., HOMO and LUMO, and their band gap (E_g) are also computed to assess the influences of interacting species on each other. The energy gap E_g is a useful parameter for determining the kinetic reactivity of materials,³⁴ and its change during the adsorption process can be used to examine the sensitivity of an adsorbent to an adsorbate.

4. RESULTS AND DISCUSSION

4.1. Structures and Energetics. As shown in Figure 1, the sulfathiazole molecule can emerge in either an imide or a thiazole form depending on the experimental conditions. Previous single crystal structure study³⁵ asserted the former with a proton residing on the ring nitrogen, is dominant in the solid state. Quantum-chemical calculations, on the contrary, predicted the latter to be more energetically stable by 1.2 kcal/mol.²¹ In this study, gas-phase calculations find that the thiazole conformation STZ_2 (Figure 3) is around 0.7 kcal/mol more stable than the imide form STZ_1 (at the PBE/cc-pVTZ level of theory). However, the energy difference turns out to be reverse in an aqueous environment as STZ_1 is now lying below STZ_2 by 2.8 kcal/mol. Thus, it appears both tautomers are likely to contribute to the population of STZ in vacuum, but in water, the imide isomer tends to dominate over its thiazole counterpart. In a vacuum, the proton affinity of STZ is computed to be around 208 kcal/mol (PBE/cc-pVTZ), being slightly larger than the corresponding value of 201 kcal/mol obtained for aniline. For this molecule, the N-sulfonamide group is more willing to interact with hydrogen ions than the N-primary amine.

In the ground state, while both Au_6 and Au_8 tend to exist in planar configurations, Au_{20} prefers a regular tetrahedron.³⁶ The Au_n clusters are expected to anchor on the STZ molecule via positions with a high electron density such as S and N atoms.

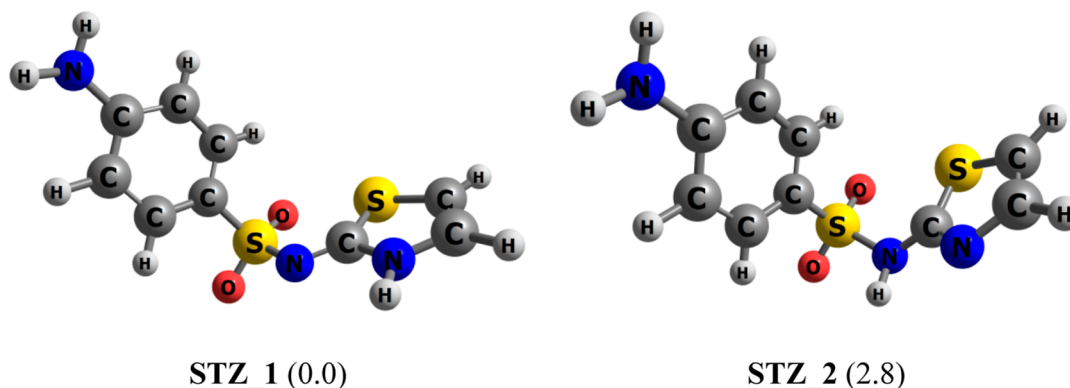


Figure 3. Equilibrium structures of two STZ lowest-energy conformations. Values in parentheses are their relative energies (kcal/mol) in aqueous solution (PBE/cc-pVTZ/IEF-PCM).

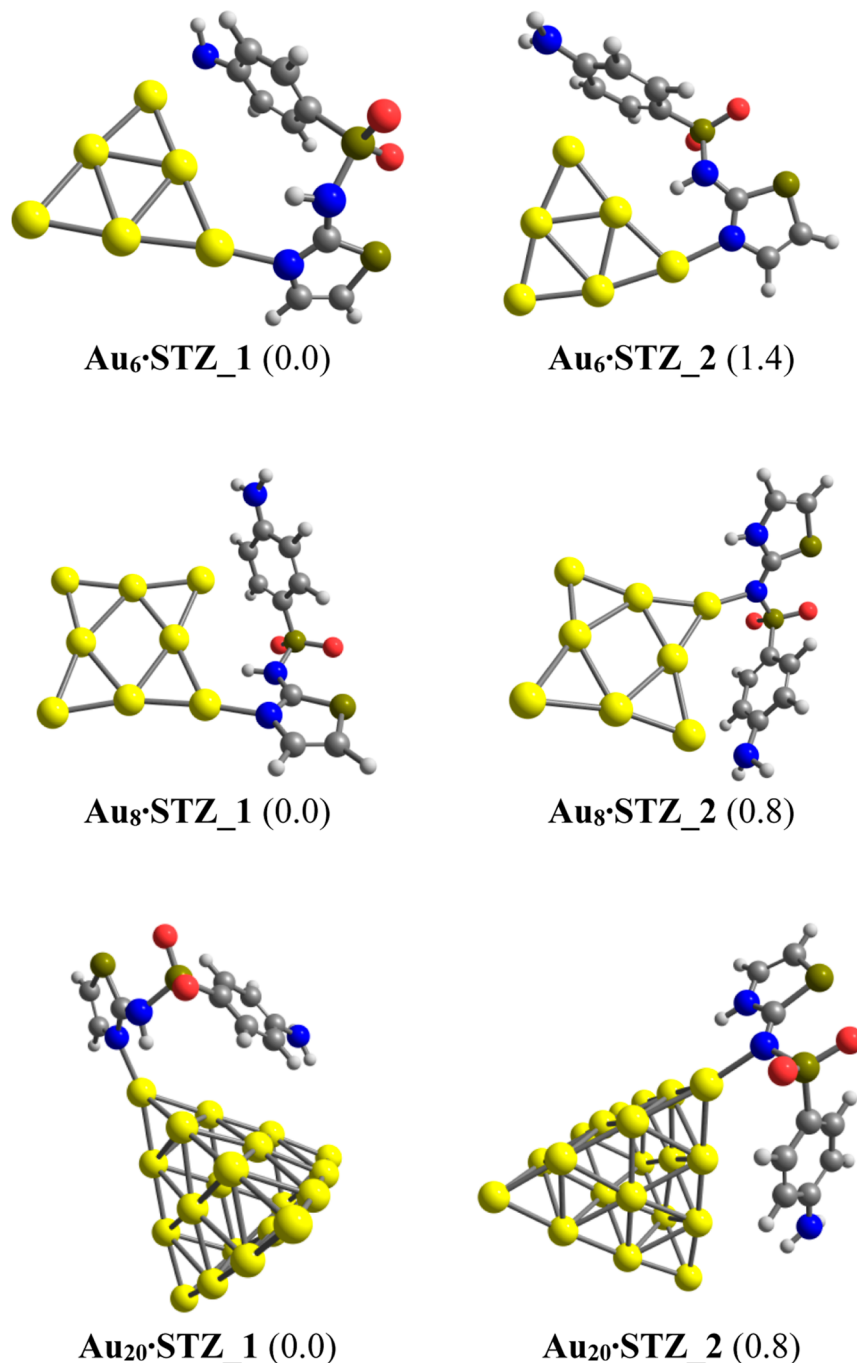


Figure 4. Lower-lying structures of the $\text{Au}_n\cdot\text{STZ}$ ($n = 6, 8, 20$) complexes obtained from PBE computations in an aqueous environment. Values given in parentheses are their relative energies (kcal/mol) with respect to the most stable form $\text{Au}_n\cdot\text{STZ}_1$.

During the interaction, the ligand is able to not only donate electron density on its lone pairs but also receive back some negative charges from the Au_n HOMO. Moreover, the metals are also willing to play as a proton acceptor by forming a weak $\text{Au}\cdots\text{H}-\text{N}$ hydrogen bond.³⁷ Previous analysis of NBO charge for Au_n clusters revealed that the cornered Au atoms are more positively charged than others^{6,38} and thus being more suitable for nucleophile attacks.

Some lowest-lying configurations located for complexes of STZ tautomers with Au_n clusters are displayed in Figure 4, while other products with higher energy are given in Figures S1–S3 of the Supporting Information file. They are denoted as

$\text{Au}_n\cdot\text{STZ}_z$ with $n = 6, 8, 20$ and $z = 1-2$ corresponding to an increasing ordering of their relative energy (RE) (kcal/mol).

In aqueous solution, gold clusters tend to anchor on STZ molecules via the nitrogen atom of the thiazole ring, giving rise to the most stable form $\text{Au}_n\cdot\text{STZ}_1$. Such forms are followed by complexes that result from directly binding Au_n clusters to the N atom of the secondary amine group. However, the energy difference between these structural motifs is negligible, being from 0.8 to 1.4 kcal/mol (Figure 4). Hence, within the expected error limit of current DFT computations, both configurations can coexist in aqueous solution, and the drug could be adsorbed on the Au surface in either imide or thiazole

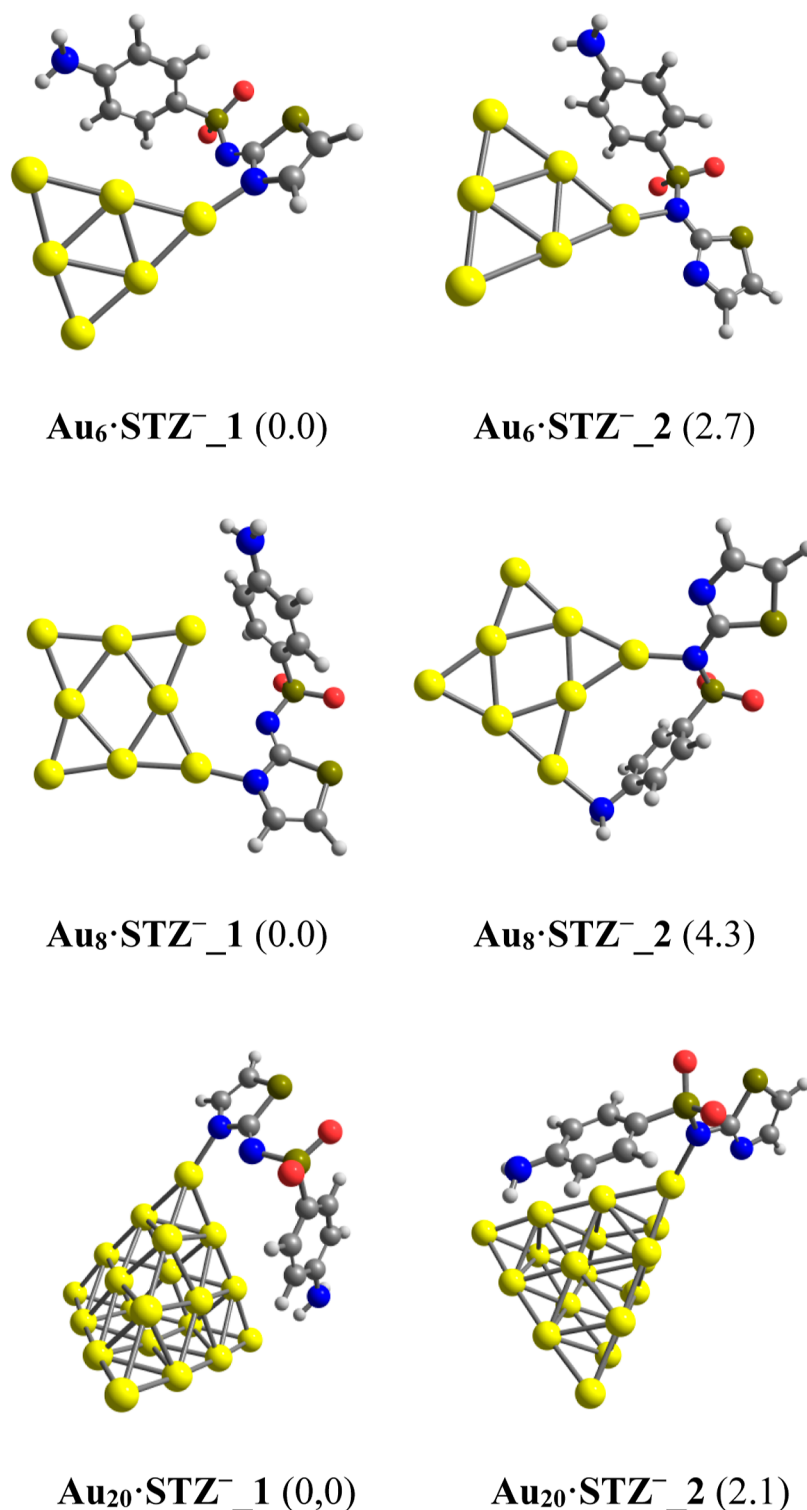


Figure 5. Lowest-energy structures located for complexes of sulfathiazole in the deprotonated form (STZ⁻) with Au_{*n*} (*n* = 6, 8, and 20) clusters. Values in parentheses are their relative energies (kcal/mol) with respect to the most stable species Au_{*n*}·STZ⁻_1.

form. In vacuum, the Au metals also tend to bind with STZ molecules via the thiazole ring nitrogen.

In addition to the thiazole-imide tautomerism, other equilibria should be taken into account in aqueous solution, such as the deprotonation. With the dissociation constants of $pK_1 = 1.9$ and $pK_2 = 7.2$,³⁹ STZ is a quite strong acid. Thus, at physiological pH or in biological environments, the drug tends to appear as a deprotonated form by the proton cleavage of

either the imide or thiazole tautomer. Such an ionic state might have a significant impact on the reactivity of STZ toward gold nanoparticles.

Some lowest-energy structures arising from Au_{*n*} clusters binding to the deprotonated form of sulfathiazole (STZ⁻) are depicted in Figure 5. Accordingly, the most stable structure of the Au_{*n*}·STZ⁻_1 complexes is formed by anchoring the Au metals on the N atom of the thiazole ring. The second most

Table 1. RE, Binding Energy (E_b), and Changes of Enthalpy (ΔH) and Gibbs Energy (ΔG) in kcal/mol for the STZ/STZ⁻ Adsorption on Gold Clusters^a

complex	RE	E_b	ΔH	ΔG	complex	RE	E_b	ΔH	ΔG
Au ₆ •STZ_1	0.0	22.4	-20.6	-6.5	Au ₆ •STZ ⁻ _1	0.0	24.6	-23.1	-11.6
Au ₆ •STZ_2	1.4	21.0	-20.4	-7.1	Au ₆ •STZ ⁻ _2	2.7	21.9	-20.6	-9.1
Au ₈ •STZ_1	0.0	28.3	-27.2	-13.2	Au ₈ •STZ ⁻ _1	0.0	35.5	-34.2	-21.3
Au ₈ •STZ_2	0.8	24.6	-22.8	-9.0	Au ₈ •STZ ⁻ _2	4.3	31.2	-29.2	-15.8
Au ₂₀ •STZ_1	0.0	17.7	-17.1	-2.2	Au ₂₀ •STZ ⁻ _1	0.0	23.0	-21.6	-9.6
Au ₂₀ •STZ_2	0.8	14.0	-12.9	-0.9	Au ₂₀ •STZ ⁻ _2	2.1	20.9	-20.1	-7.1

^aSimulations are performed in an aqueous solvent.

stable conformation, i.e., Au_{*n*}•STZ⁻_2, which is generated by anchoring the secondary amine nitrogen on Au_{*n*}, is around 2–4 kcal/mol higher in energy (Figure 5). Overall, the deprotonated form of STZ also prefers binding to Au metals through the thiazole nitrogen over the secondary amine one. In addition, the resulting complexes are further stabilized by a ring-surface π interaction between the benzene ring of STZ moiety and the Au surface.

Binding energy (E_b) along with changes of enthalpy and Gibbs energy (ΔG) for the adsorption processes are also computed to evaluate the strength of interactions between the STZ molecules with gold clusters (Table 1). In an aqueous environment, both tautomers of STZ overall exhibit a significantly different affinity toward Au metals. For example, the binding energies of the thiazole form with Au₆ are computed to be around 22 kcal/mol, and greatly increase to 28 kcal/mol for Au₈, as compared to the corresponding values of 16 and 25 kcal/mol obtained for the imide form. In vacuum, thiazole conformation STZ_2 also exhibits a higher affinity with Au metals than its counterpart STZ_1. Indeed, the gas-phase E_b values of STZ_1 and STZ_2 with Au₈ are about 29 and 33 kcal/mol, respectively, while such values in Au₆•STZ adducts correspond to 22 and 24 kcal/mol (Table 1). As expected the higher reactivity of Au₈ toward the drug molecules as compared to that of Au₆ and Au₂₀ correlates well with its smaller band gap and lower stability.³⁶ When the entropic effect is included, such energetic parameters turn out to be smaller, but a similar tendency is still observed. For the most stable Au_{*n*}•STZ_1 complexes in aqueous solution, the Gibbs energies are calculated to be about -7 and -13 kcal/mol for $n = 6$ and 8, respectively, as compared to the corresponding E_b values of 22 and 28 kcal/mol. The smaller absolute values of Gibbs energies can be understood by the fact that the entropy tends to decrease during the adsorption process.

In order to include the dispersion corrections, we performed further computations using the PBE-D3 functional with the cc-pVDZ-PP/cc-pVTZ basis set. Computed results summarized in Table S5 (Supporting Information) reveal that the binding energies between the gold cluster and the STZ molecule turn out to be much larger upon inclusion of dispersion. For example, the binding energy of Au₆•STZ obtained with PBE-D3 is 31 kcal/mol as compared to a PBE value of 22.4 kcal/mol. (Table S5 of the Supporting Information). The basis set superposition error (BSSE) corrections are also computed and are presented in Table S6 (Supporting Information). Accordingly, its contribution to the final binding energy is computed to be around 2–3 and 3–4 kcal/mol for Au_{*n*} interacting with the neutral STZ and the anion STZ⁻, respectively.

As compared to its neutral form, deprotonated state STZ⁻ exhibits a quite higher affinity toward gold nanoparticles. Indeed, the absolute values of both binding and free Gibbs energies turn out to be larger, indicating that the interaction becomes stronger and the resulting complexes are more stable. For instance, the E_b and ΔG values for forming Au₂₀•STZ⁻_1 are computed to be 23 and -10 kcal/mol, respectively, as compared to the corresponding values of 18 and -2 kcal/mol obtained for Au₂₀•STZ_1 (Table 1).

The equilibrium Au–N distances in Au_{*n*}•STZ_1 complexes are predicted to be 2.18, 2.16, and 2.22 Å for $n = 6, 8,$ and 20, respectively. Basically, a shorter Au–N bond length reflects a stronger interaction. The equilibrium distances thus correlate well with the interaction energies. The Au–N bond length around 2.14 Å in Au₆•STZ⁻_1 turns out to be much shorter than the corresponding value of 2.18 Å in the complex of Au₆ with free STZ. In addition, the Au–N distances in these complexes are comparable to the sum of the covalent radii of Au (1.44 Å) and N (0.75 Å) atoms.⁴⁰ Such results manifest the effectiveness of the interactions between the drug and Au metals, which could be observed by spectroscopic techniques.

4.2. SERS Chemical Enhancement of Sulfathiazole by Gold Nanoparticles. The SERS technique is a popular analytical approach for the characterization of adsorption processes on metal surfaces. As adsorbed on nanostructured surfaces, the Raman signatures of organic compounds are substantially enhanced and turn out to be much more easily identified. In practice, the SERS signals have been widely used to detect and/or clarify the adsorption behavior of various molecules on metallic nanoparticles.⁷ Moreover, of several spectroscopic approaches established to detect residues at trace concentrations, the SERS method has attracted great interest from the scientific community and becomes more and more popular in biosensing and molecular imaging.^{41,42} Owing to striking advantages including rapid-detection, simple-operation and high-sensitivity, such techniques have been extensively used to determinate trace antibiotics.⁴³

In order to interpret the SERS phenomenon, two key mechanisms, namely, the chemical and electromagnetic enhancements, are normally taken into consideration.^{44,45} In the latter mechanism, certain Raman modes of molecules in close vicinity of the metallic surface get greatly enhanced as the Raman intensity directly correlates with the squared local electromagnetic field intensity.⁴⁶ In addition, the Raman-scattered light may excite an extra enhancement when the Raman signals couple with the plasmonic resonance.⁴⁷ The former mechanism, on the other hand, is basically related to a chemical interaction and a charge flow between adsorbed molecules and nanoparticles.⁴⁸ Overall, vibrational modes parallel to the metallic surfaces are predicted to induce negligible enhancements.

Normal Raman signatures located at peaks below 1700 cm^{-1} of both **STZ_1** and **STZ_2** tautomers along with the deprotonated form of **STZ⁻** simulated in an aqueous solution are depicted in Figure 6. Accordingly, several significant signals

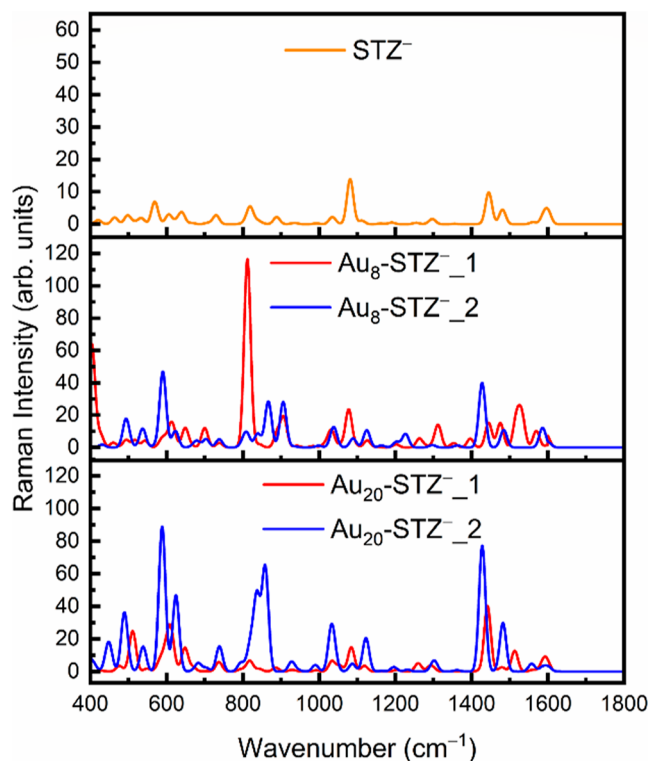


Figure 6. Normal Raman signatures of **STZ⁻** anion and its SERS spectra on Au_n ($n = 8, 20$) surfaces. Simulations are carried out in an aqueous environment.

are located at around $600, 650, 825, 1090,$ and 1600 cm^{-1} for the free molecule. Similarly, several highly intense peaks at $\sim 605, 640, 820, 1080, 1450,$ and 1600 cm^{-1} can also be observed on the Raman spectrum of the anion **STZ⁻**. Overall, it is rather difficult to definitely assign the vibrational modes in this energy region as they normally give rise from a combination of some vibrations including ring deformation, C–X ($X = \text{S}, \text{N}$) stretches, and Y–H ($Y = \text{C}, \text{N}$) deflections. For example, strong peaks around $600\text{--}650\text{ cm}^{-1}$ likely result from a coupling of the ring distortion with C–N bending modes. Meanwhile, the ring breathing along with N–S stretching and C–H bending modes results in typical signals in the region of $800\text{--}830\text{ cm}^{-1}$. On the contrary, the rather sharp bands near 1100 cm^{-1} are mostly due to the combination of C–C and S–O stretching modes. Previously, such vibrations were experimentally observed at $641, 832,$ and 1072 cm^{-1} and accordingly assigned to the ring breathing, along with C–S and C–N stretching modes, respectively.^{21,22}

The simulated SERS spectra of the deprotonated **STZ⁻** form adsorbed on Au_n clusters with $n = 8$ and 20 are displayed in Figure 6, while the SERS spectra of the neutral molecule are given in Figure S4 of the Supporting Information file. In the SERS spectra of $\text{Au}_8\cdot\text{STZ}^-$ complexes, the most enhanced signal is located near 810 cm^{-1} , mainly resulting from the C–H bending modes of the benzene ring. Such an enhancement is likely due to a ring-surface π interaction⁴⁹ as the benzene ring of the drug is almost lying parallel to the gold surfaces. On the

contrary, the SERS spectra of **STZ⁻** on the Au_{20} are characterized by the most enhanced peak near 1450 cm^{-1} . From a methodological viewpoint, the use of the Au_{20} cluster size as a simple model to mimic the nanoparticle surface is likely appropriate to reproduce the experimental results better than that of the smaller size Au_8 .

A comparison of the Raman signatures simulated in different environments allows us to figure out some deviations in the band positions and intensities. Basically, although the intensities are significantly modified, the spectral positions remain almost unchanged. In particular, the SERS intensities of $\text{Au}_{20}\cdot\text{STZ}$ are much weaker in comparison to those of $\text{Au}_{20}\cdot\text{STZ}^-$. The anion, in addition, appears to exhibit a much higher affinity with Au than the neutral. During the preparation of the SERS sample, the average pH is controlled approximately at 6.5. Therefore, the dominant species in the SERS spectra is likely the anion **STZ⁻**. In this regard, we focus on the SERS signatures of $\text{Au}_{20}\cdot\text{STZ}^-$ complexes as the representative model.

As shown in Figure 6, several peaks centered at $600, 650, 850, 1050, 1130, 1440,$ and 1540 cm^{-1} are significantly enhanced when the anion **STZ⁻** is adsorbed on the Au_{20} surface. The simulated SERS signals at $1050, 1130, 1430,$ and 1540 cm^{-1} could be assigned to the experimental ones observed at $1075, 1142, 1445,$ and 1585 cm^{-1} , respectively (cf. the experimental spectrum in Figure 2). The most enhanced band near 1430 cm^{-1} in the calculated SERS spectrum of $\text{Au}_{20}\cdot\text{STZ}^-_1$ arises mainly from the C–N stretching modes, as these vibrations are directly oriented to Au atoms. On the contrary, the peak above 1550 cm^{-1} that was previously selected to detect the presence of **STZ** is likely to result from a coupling of some vibrations including the ring breathing, C–C stretching, and N–H bending.

As a result of a charge transfer (CT) process between the metal and the adsorbate, some relevant intensity should be located near 1600 cm^{-1} corresponding to the benzene ring stretches.⁵⁰ In order to test out the validity of such an enhancement mechanism, the Raman spectrum of the **STZ^{*2-}** radical dianion is simulated and presented in Figure S5 of the SI. Accordingly, an enhanced signal near 1600 cm^{-1} in the calculated Raman spectrum of **STZ^{*2-}** is mostly missing. This observation indicates that the 1600 cm^{-1} band in the experimental SERS spectrum is likely to be enhanced through non-CT mechanisms such as electromagnetic enhancement. However, an appropriate treatment of this issue goes beyond the scope of the present study.

4.3. Electronic Properties and Binding Mechanism.

To obtain deeper insights into the interaction mechanism, the energy levels of frontier orbitals, i.e., HOMO and LUMO, in the antibiotic, Au_n clusters, and the resulting complexes are also considered. The change of HOMO–LUMO energy gap (ΔE_g) is computed following eq 4

$$\Delta E_g = \frac{|E_{g_2} - E_{g_1}|}{E_{g_1}} \times 100\% \quad (4)$$

where E_{g_1} and E_{g_2} are the band gaps of gold clusters and $\text{Au}_n\cdot\text{STZ}$ complexes, respectively.

The change of E_g value is a helpful indicator for recognizing the presence of adsorbents on a metal surface.⁵¹ Indeed, a decrease of E_g results in an exponential increase of the electrical conductivity (σ) of a material,⁵² as described in eq 5

Table 2. Energy Levels of HOMO and LUMO, Energy Gap (E_g), and Change of Energy Gap (ΔE_g) upon the Drug Adsorption on the Au_n ($n = 6, 8,$ and 20) Clusters^a

species	in vacuum				in water			
	HOMO	LUMO	E_g	ΔE_g	HOMO	LUMO	E_g	ΔE_g
Au_6	-5.9	-3.9	2.0		-5.4	-3.1	2.3	
Au_8	-5.8	-4.4	1.4		-5.3	-3.7	1.6	
Au_{20}	-5.7	-3.9	1.8		-5.1	-3.2	1.9	
STZ_1	-5.4	-1.9	3.4		-5.4	-2.0	3.4	
STZ_2	-5.0	-1.5	3.5		-5.1	-1.8	3.3	
STZ ⁻					-4.4	-1.3	3.1	
$Au_6 \cdot STZ_1$	-4.8	-3.1	1.7	-15.0	-4.9	-3.0	1.9	-17.4
$Au_8 \cdot STZ_1$	-5.1	-3.5	1.6	14.3	-5.1	-3.4	1.7	6.3
$Au_{20} \cdot STZ_1$	-5.4	-3.8	1.6	-12.8	-4.8	-3.2	1.7	-11.6
$Au_6 \cdot STZ^-_1$					-4.8	-2.9	1.9	-17.4
$Au_8 \cdot STZ^-_1$					-4.8	-3.3	1.5	-6.3
$Au_{20} \cdot STZ^-_1$					-4.7	-3.2	1.6	-17.7

^aThe results are obtained at the PBE/cc-pVTZ/cc-pVDZ-PP level and are given in eV, except for ΔE_g (%).

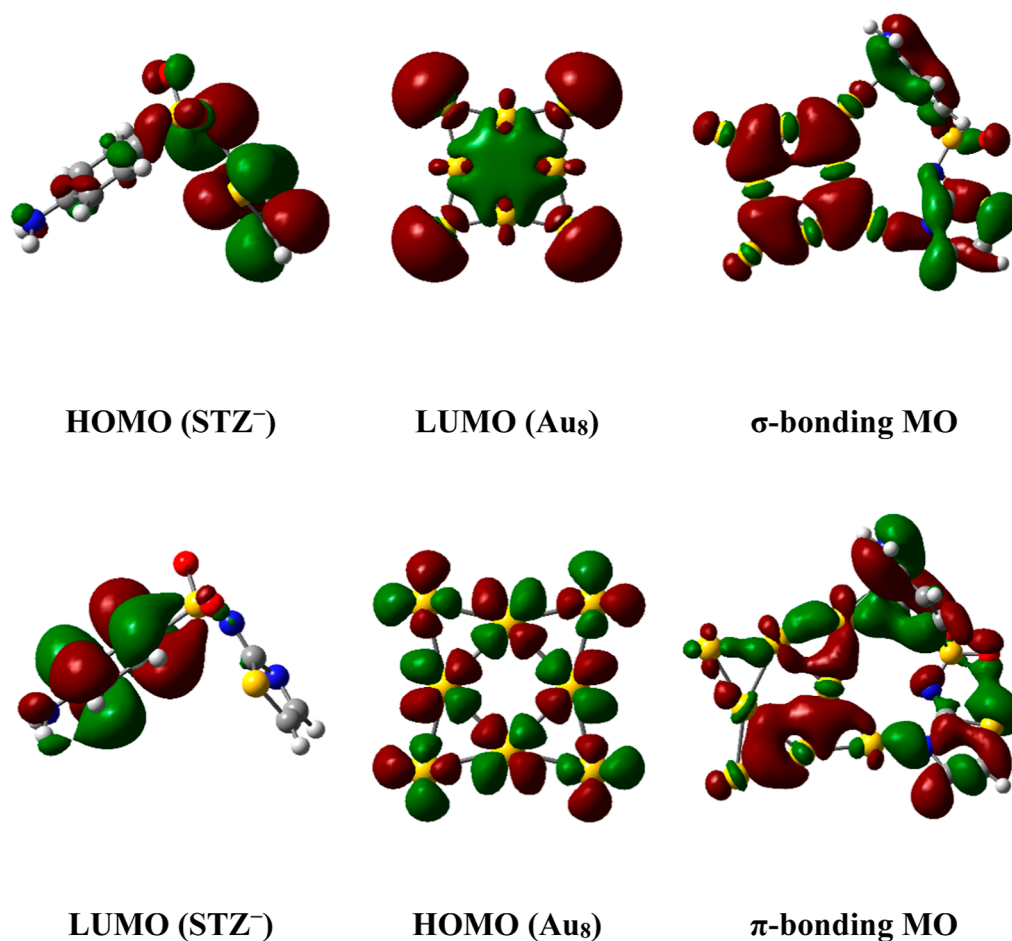


Figure 7. Shapes of frontier orbitals of Au_8 cluster and the anion STZ^- before and after interaction (the isovalue for orbital contours is 0.02).

$$\sigma = AT^{3/2} e^{-E_g/2k_B T} \quad (5)$$

where A is a constant, k_B being the Boltzmann's constant, and T being the thermodynamic temperature. Hence, a slight alteration of E_g during an adsorption is expected to induce a significant change of electric conductivity of the system.

The band gaps of Au_6 calculated with the PBE functional are about 2.0 and 2.3 eV in a vacuum and water, respectively. For Au_8 , the corresponding values are greatly reduced to 1.4 eV in a vacuum and 1.6 eV in water. As listed in Table 2, the E_g value

of Au_6 is substantially decreased due to the adsorption of both STZ and STZ^- . Accordingly, the band gap of Au_6 is predicted to decline by 17.4% in both gas-phase and aqueous environments. However, such a change for the adsorption on Au_8 is likely to be lesser and inconsistent, i.e., increasing for binding with STZ, but decreasing for binding with STZ^- . As mentioned above, a small reduction of E_g also results in an enormous increase in the electrical conductivity that is feasibly

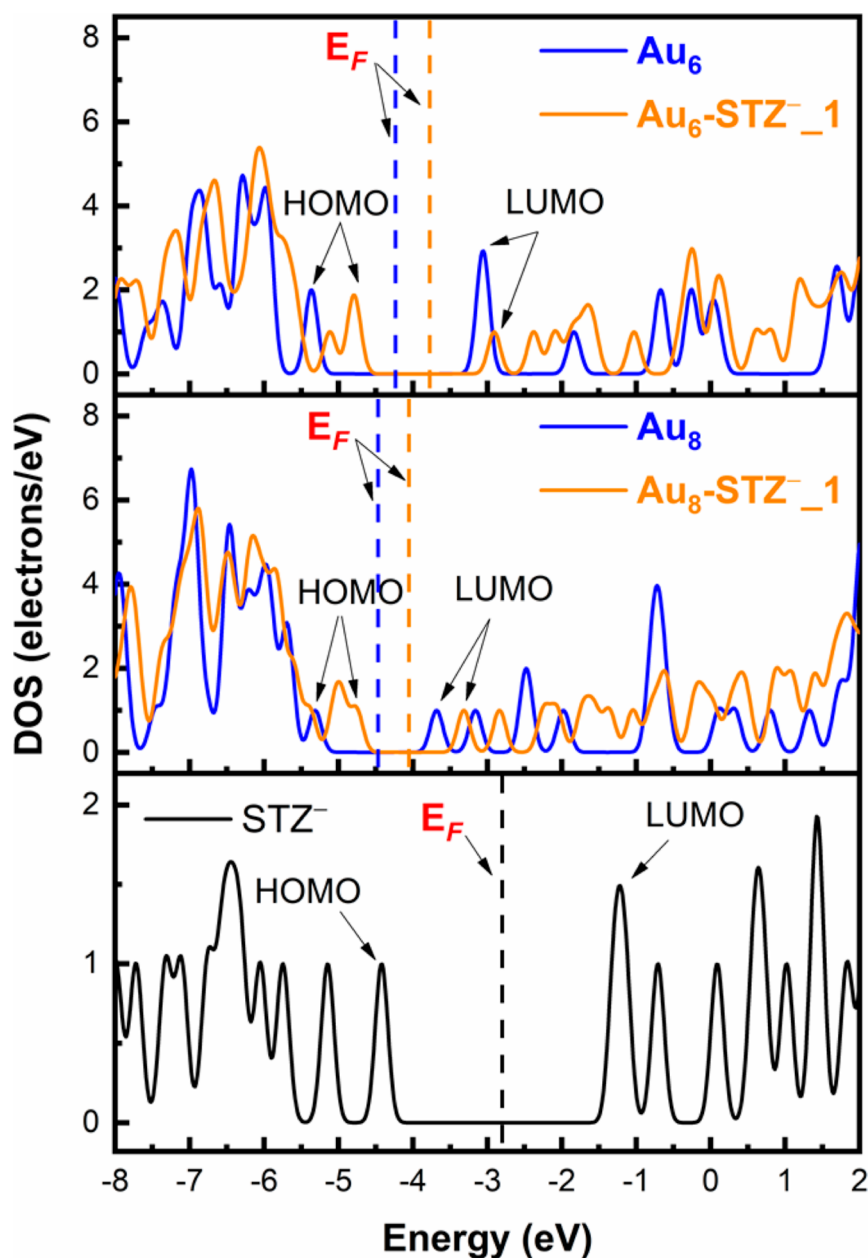


Figure 8. Density of states of the $\text{Au}_6\text{:STZ}^-_1$ and $\text{Au}_8\text{:STZ}^-_1$ complexes. The Fermi levels are denoted as vertical dash lines.

converted into an electrical noise, allowing us to identify the drug presence.

The energy and symmetry of frontier orbitals are among the most relevant features to be used to examine the electronic structures of metal clusters and their related properties. The energy difference between HOMO and LUMO, i.e., the band gap, is often used as a pointer to assess the electrical conductivity and the kinetic and chemical stability of metal clusters.⁵³ As given in Table 2, a smaller HOMO–LUMO gap of Au_8 correlates well with its higher reactivity toward the drug compared to Au_6 . Similarly, the anionic state STZ^- with a smaller E_g value also has a higher affinity with gold metals than the neutral form STZ. Moreover, information from frontier orbitals could provide us with more profound insights into the mechanism of interaction between the Au metals and the drug molecules. The combination related to the LUMO and the HOMO orbitals of the Au metals and those of the STZ moiety

is virtually the most important factor. Accordingly, dependent on their energy difference and symmetry, either forward or backward donation will be more prevailing.

In aqueous solution, the energy difference between the LUMO of STZ molecule and the HOMO of Au_n ($n = 6, 8$) species is around 3.5 eV, whereas the gap between gold clusters (LUMO) and STZ molecule (HOMO) is reduced to 2.0 eV (Table 2). Such values are predicted to be around 4.0 and 1.0 eV, respectively, for anion STZ^- . The energy gap LUMO–HOMO of the backward donation ($\text{Au}_n \rightarrow \text{STZ}$) is thus much larger than that of the forward donation ($\text{STZ} \rightarrow \text{Au}_n$). Therefore, the interaction between these compounds is mostly characterized by the latter process $\text{STZ} \rightarrow \text{Au}_n$, in which the drug tends to act as an electron donor and the Au metals play a role as an electron acceptor. Moreover, due to a smaller LUMO–HOMO of the $\text{STZ}^- \rightarrow \text{Au}_n$ forward donation as compared to the $\text{STZ} \rightarrow \text{Au}_n$ process, the anion STZ^- turns

out to interact with the gold clusters more strongly than its neutral state. The CTs in $\text{Au}_{20}\cdot\text{STZ}^-_1$ and $\text{Au}_{20}\cdot\text{STZ}^-_1$ complexes, which are further illustrated in Figure S6 of the Supporting Information, point out that a charge flow occurs from the ligands to the metals. Accordingly, in both complexes, while Au_{20} becomes blue, STZ/STZ^- turns out to be green, implying an increase of the electron density on Au_{20} and a decrease of the electron density on STZ/STZ^- .

As shown in Figure 7, the LUMO of Au_8 cluster interacts well with the HOMO of STZ^- anion, giving rise to a σ -type bonding orbital. In addition, the LUMO of STZ^- can also overlap with the HOMO of Au_8 , forming a π -type bonding orbital. Nonetheless, the forward donation still plays a much greater role than the backward interaction, and it is expected that there also exists a charge flow from the ligand to Au metals. This can be understood on the basis of the density of states (DOS) of relevant species. The plots of DOS for Au_n clusters and STZ^- anion are depicted in Figure 8. Accordingly, the HOMO and LUMO energy levels of both the STZ^- and Au_n systems are substantially modified during complex formation.

First, one can observe the fading of the signal related to the STZ^- lone pair around -4.3 eV in the DOS of the $\text{Au}_n\cdot\text{STZ}^-$ complexes. This obviously denotes that the ligand is binding to the Au surface by partially donating some electron density to the metals. For $\text{Au}_6\cdot\text{STZ}^-_1$, both LUMO and HOMO levels of Au_6 shift to the more positive energy region, in which the latter undergoes a more significant one. Consequently, the band gap of Au_6 is decreased by $\sim 17\%$ (PBE value). Regarding $\text{Au}_8\cdot\text{STZ}^-_1$, both LUMO and HOMO levels of Au_8 also shift to the higher energy region, but the changes are somewhat comparable to each other. Therefore, the E_g value of Au_8 is declined by a smaller extent (6%) following interaction. The decrease in the band gap during the adsorption may result in an alteration of fluorescence emission which can be employed as an indicator to detect the drug presence by relevant spectrophotometers.

5. CONCLUDING REMARKS

In this combined theoretical and experimental study, the adsorption behavior of sulfathiazole (STZ), a powerful antibiotic for the prevention and cure of bacterial infections, on gold nanoparticles is elucidated by means of quantum chemical calculations and SERS techniques. The most preferred binding mode is formed by anchoring Au metals to the nitrogen of the thiazole ring. The interaction is further stabilized by the ring-surface π coupling, with the benzene ring almost parallel to the gold surface. As a rather strong acid, the drug molecule tends to exist as a deprotonated form in aqueous or biological environments. With the binding energies in the range of 25 to 36 kcal/mol, the anion STZ^- is found exhibit a greater affinity toward Au nanoparticles as compared to its neutral form STZ.

The band gap of Au metals is also adjusted due to the drug adsorption, which is expected to induce a change of optical properties. Analysis based on frontier orbitals reveals that the forward donation from the HOMO of STZ to LUMO of Au_n constitutes the main contribution for the Au–STZ bonding formation. Several SERS signals are identified at 1050, 1130, 1430, and 1540 cm^{-1} that can be assigned to the experimentally observed bands at 1075, 1142, 1445, and 1585 cm^{-1} , respectively. In particular, the most enhanced band above 1400 cm^{-1} is due to the C–N stretching modes that are

directly oriented toward the Au surface. Another significant enhancement near 1550 cm^{-1} , on the contrary, results from a coupling of several vibrations including the ring breathing, C–C stretching, and N–H bending. Such Raman characteristic signals can be employed for both qualitative detection and quantitative assessment of the STZ drug molecule at trace concentration.

■ ASSOCIATED CONTENT

Supporting Information

The Supporting Information is available free of charge at <https://pubs.acs.org/doi/10.1021/acsomega.3c01477>.

Geometries of low-lying structures of the $\text{Au}_n\cdot\text{STZ}$ ($n = 6, 8, \text{ and } 20$) complexes and their Cartesian coordinates and different calculated energies (PDF)

■ AUTHOR INFORMATION

Corresponding Authors

Minh Tho Nguyen – Laboratory for Chemical Computation and Modeling, Institute for Computational Science and Artificial Intelligence, Van Lang University, Ho Chi Minh City 70000, Vietnam; Faculty of Applied Technology, School of Technology, Van Lang University, Ho Chi Minh City 70000, Vietnam; orcid.org/0000-0002-3803-0569; Email: minhtho.nguyen@vlu.edu.vn

Pham Vu Nhat – Department of Chemistry, Can Tho University, Can Tho City 90000, Vietnam; Molecular and Materials Modeling Laboratory, Can Tho University, Can Tho City 90000, Vietnam; orcid.org/0000-0002-1485-6569; Email: nhat@ctu.edu.vn

Authors

Tran Ni Kha – Department of Chemistry, Can Tho University, Can Tho City 90000, Vietnam

Nguyen Thanh Si – Department of Chemistry, Can Tho University, Can Tho City 90000, Vietnam; Institute of Environmental Science and Technology, Tra Vinh University, Tra Vinh City 94000, Vietnam

Van Man Tran – Faculty of Chemistry, University of Science, Vietnam National University, Ho Chi Minh City 70000, Vietnam

Khuong Quoc Vo – Faculty of Chemistry, University of Science, Vietnam National University, Ho Chi Minh City 70000, Vietnam

Complete contact information is available at:

<https://pubs.acs.org/doi/10.1021/acsomega.3c01477>

Notes

The authors declare no competing financial interest.

■ ACKNOWLEDGMENTS

The work of P.V.N., N.T.S., and M.T.N. is funded by VinGroup (Vietnam) and supported by VinGroup Innovation Foundation (VinIF) under project code VinIF.2020.DA21. M.T.N. thanks Van Lang University for support.

■ REFERENCES

(1) Samuel, Y.; Garg, A.; Mulugeta, E. Synthesis, DFT analysis, and evaluation of antibacterial and antioxidant activities of sulfathiazole derivatives combined with *in silico* molecular docking and ADMET predictions. *Biochem. Res. Int.* **2021**, *2021*, 7534561.

- (2) Muthu Prabhu, A. A.; Venkatesh, G.; Rajendiran, N. Spectral characteristics of sulfa drugs: effect of solvents, pH and β -cyclodextrin. *J. Solution Chem.* **2010**, *39* (7), 1061–1086.
- (3) Wen, Y.; Zhang, M.; Zhao, Q.; Feng, Y.-Q. Monitoring of five sulfonamide antibacterial residues in milk by in-tube solid-phase microextraction coupled to high-performance liquid chromatography. *J. Agric. Food Chem.* **2005**, *53* (22), 8468–8473.
- (4) Bellú, S.; Hure, E.; Trapé, M.; Rizzotto, M.; Sutich, E.; Sigrist, M.; Moreno, V. The interaction between mercury (II) and sulfathiazole. *Quím. Nova* **2003**, *26*, 188–192.
- (5) Goodman, L. S. *Goodman and Gilman's the pharmacological basis of therapeutics*; McGraw-Hill New York, 1996; Vol. 1549.
- (6) Nhat, P. V.; Si, N. T.; Tram, N. T. T.; Duong, L. V.; Nguyen, M. T. Elucidating the binding mechanism of thione containing mercaptopurine and thioguanine drugs to small gold clusters. *J. Comput. Chem.* **2020**, *41* (19), 1748–1758.
- (7) Vu Nhat, P.; Si, N. T.; Tien, N. T.; Nguyen, M. T. Theoretical study of the binding of the thiol-containing cysteine amino acid to the silver surface using a cluster model. *J. Phys. Chem. A* **2021**, *125* (16), 3244–3256.
- (8) Si, N. T.; Nhung, N. T. A.; Bui, T. Q.; Nguyen, M. T.; Nhat, P. V. Gold nanoclusters as prospective carriers and detectors of pramipexole. *RSC Adv.* **2021**, *11* (27), 16619–16632.
- (9) Hang, N. T. N.; Si, N. T.; Nguyen, M. T.; Nhat, P. V. Adsorption/desorption behaviors and SERS chemical enhancement of 6-mercaptopurine on a nanostructured gold surface: The Au₂₀ cluster model. *Molecules* **2021**, *26* (17), 5422.
- (10) Hola, K.; Markova, Z.; Zoppellaro, G.; Tucek, J.; Zboril, R. Tailored functionalization of iron oxide nanoparticles for MRI, drug delivery, magnetic separation and immobilization of biosubstances. *Biotechnol. Adv.* **2015**, *33* (6), 1162–1176.
- (11) Wei, L.; Lu, J.; Xu, H.; Patel, A.; Chen, Z.-S.; Chen, G. Silver nanoparticles: synthesis, properties, and therapeutic applications. *Drug Discovery Today* **2015**, *20* (5), 595–601.
- (12) Borker, S.; Patole, M.; Moghe, A.; Pokharkar, V. Engineering of pectin-reduced gold nanoparticles for targeted delivery of an antiviral drug to macrophages: in vitro and in vivo assessment. *Gold Bull.* **2017**, *50* (3), 235–246.
- (13) Hainfeld, J. F.; Slatkin, D. N.; Focella, T. M.; Smilowitz, H. M. Gold nanoparticles: A new X-ray contrast agent. *Br. J. Radiol.* **2006**, *79*, 248–253.
- (14) Fratoddi, I.; Venditti, I.; Cametti, C.; Russo, M. V. How toxic are gold nanoparticles? The state-of-the-art. *Nano Res.* **2015**, *8* (6), 1771–1799.
- (15) Kumar, A.; Zhang, X.; Liang, X.-J. Gold nanoparticles: emerging paradigm for targeted drug delivery system. *Biotechnol. Adv.* **2013**, *31* (5), 593–606.
- (16) Casals, E.; Pfaller, T.; Duschl, A.; Oostingh, G. J.; Puentes, V. Time evolution of the nanoparticle protein corona. *ACS Nano* **2010**, *4* (7), 3623–3632.
- (17) Wang, C.; Zhang, H.; Zeng, D.; San, L.; Mi, X. DNA nanotechnology mediated gold nanoparticle conjugates and their applications in biomedicine. *Chin. J. Chem.* **2016**, *34* (3), 299–307.
- (18) Khalil, I.; Julkapli, N. M.; Yehye, W. A.; Basirun, W. J.; Bhargava, S. K. Graphene-gold nanoparticles hybrid—synthesis, functionalization, and application in an electrochemical and surface-enhanced raman scattering biosensor. *Materials* **2016**, *9* (6), 406.
- (19) Kong, F.-Y.; Zhang, J.-W.; Li, R.-F.; Wang, Z.-X.; Wang, W.-J.; Wang, W. Unique roles of gold nanoparticles in drug delivery, targeting and imaging applications. *Molecules* **2017**, *22* (9), 1445.
- (20) Fatima, A.; Pooja, K.; Savita, S.; Singh, M.; Verma, I.; Siddiqui, N.; Javed, S. Quantum chemical, experimental spectroscopic, Hirshfeld surface and molecular docking studies of the anti-microbial drug Sulfathiazole. *J. Mol. Struct.* **2021**, *1245*, 131118.
- (21) Ratkaj, M.; Miljanić, S. Adsorption mechanisms of sulfathiazole on gold, silver and copper surfaces studied by SERS. *Vib. Spectrosc.* **2014**, *74*, 104–109.
- (22) Xu, L.; Wu, R.; Geng, X.; Zhu, X.; Xiong, Y.; Chen, T.; Ai, S. Rapid detection of sulfonamide antibiotics residues in swine urine by surface-enhanced Raman spectroscopy. *Spectrochim. Acta, Part A* **2022**, *267*, 120570.
- (23) Kawamura, G.; Nogami, M. Application of a conproportionation reaction to a synthesis of shape-controlled gold nanoparticles. *J. Cryst. Growth* **2009**, *311* (19), 4462–4466.
- (24) Turkevich, J.; Stevenson, P. C.; Hillier, J. A study of the nucleation and growth processes in the synthesis of colloidal gold. *Discuss. Faraday Soc.* **1951**, *11* (0), 55–75.
- (25) Hu, Y.; Erxleben, A.; Ryder, A. G.; McArdle, P. Quantitative analysis of sulfathiazole polymorphs in ternary mixtures by attenuated total reflectance infrared, near-infrared and Raman spectroscopy. *J. Pharm. Biomed. Anal.* **2010**, *53* (3), 412–420.
- (26) Ali, H. R. H.; Edwards, H. G. M.; Scowen, I. J. Insight into thermally induced solid-state polymorphic transformation of sulfathiazole using simultaneous in situ Raman spectroscopy and differential scanning calorimetry. *J. Raman Spectrosc.* **2009**, *40* (8), 887–892.
- (27) Topaçli, C.; Topaçli, A. Ab initio calculations and vibrational structure of sulfanilamide. *J. Mol. Struct.* **2003**, *644* (1–3), 145–150.
- (28) Ruedas Rama, M. J.; López-Sánchez, M.; Ruiz-Medina, A.; Molina-Díaz, A.; Ayora-Cañada, M. J. Flow-through sensor with Fourier transform Raman detection for determination of sulfonamides. *Analyst* **2005**, *130* (12), 1617–1623.
- (29) Frisch, M. J.; Trucks, G. W.; Schlegel, H. B.; Scuseria, G. E.; Robb, M. A.; Cheeseman, J. R.; Scalmani, G.; Barone, V.; Petersson, G. A.; Nakatsuji, H.; Li, X.; Caricato, M.; Marenich, A. V.; Bloino, J.; Janesko, B. G.; Gomperts, R.; Mennucci, B.; Hratchian, H. P.; Ortiz, J. V.; Izmaylov, A. F.; Sonnenberg, J. L.; Williams Ding, F.; Lipparini, F.; Egidi, F.; Goings, J.; Peng, B.; Petrone, A.; Henderson, T.; Ranasinghe, D.; Zakrzewski, V. G.; Gao, J.; Rega, N.; Zheng, G.; Liang, W.; Hada, M.; Ehara, M.; Toyota, K.; Fukuda, R.; Hasegawa, J.; Ishida, M.; Nakajima, T.; Honda, Y.; Kitao, O.; Nakai, H.; Vreven, T.; Throssell, K.; Montgomery, J. A., Jr.; Peralta, J. E.; Ogliaro, F.; Bearpark, M. J.; Heyd, J. J.; Brothers, E. N.; Kudin, K. N.; Staroverov, V. N.; Keith, T. A.; Kobayashi, R.; Normand, J.; Raghavachari, K.; Rendell, A. P.; Burant, J. C.; Iyengar, S. S.; Tomasi, J.; Cossi, M.; Millam, J. M.; Klene, M.; Adamo, C.; Cammi, R.; Ochterski, J. W.; Martin, R. L.; Morokuma, K.; Farkas, O.; Foresman, J. B.; Fox, D. J. *Gaussian 16 Rev. C.01*; Gaussian, Inc.: Wallingford, CT, 2019.
- (30) Perdew, J. P.; Burke, K.; Ernzerhof, M. Generalized gradient approximation made simple. *Phys. Rev. Lett.* **1996**, *77* (18), 3865–3868.
- (31) Peterson, K. A. Systematically convergent basis sets with relativistic pseudo-potentials. I. Correlation consistent basis sets for the post-d group 13–15 elements. *J. Chem. Phys.* **2003**, *119* (21), 11099–11112.
- (32) Tomasi, J.; Mennucci, B.; Cammi, R. Quantum mechanical continuum solvation models. *Chem. Rev.* **2005**, *105* (8), 2999–3094.
- (33) Ochterski, J. W. *Thermochemistry in Gaussian*, 2000. see: help@gaussian.com.
- (34) Hadipour, N. L.; Ahmadi Peyghan, A.; Soleymanabadi, H. Theoretical study on the Al-doped ZnO nanoclusters for CO chemical sensors. *J. Phys. Chem. C* **2015**, *119* (11), 6398–6404.
- (35) Gelbrich, T.; Hughes, D. S.; Hursthouse, M. B.; Threlfall, T. L. Packing similarity in polymorphs of sulfathiazole. *CrystEngComm* **2008**, *10* (10), 1328–1334.
- (36) Nhat, P. V.; Si, N. T.; Leszczynski, J.; Nguyen, M. T. Another look at structure of gold clusters Au_n from perspective of phenomenological shell model. *Chem. Phys.* **2017**, *493*, 140–148.
- (37) Pakiari, A. H.; Jamshidi, Z. Interaction of amino acids with gold and silver clusters. *J. Phys. Chem. A* **2007**, *111*, 4391–4396.
- (38) Nhat, P. V.; Nguyen, P. T. N.; Si, N. T. A computational study of thiol-containing cysteine amino acid binding to Au₆ and Au₈ gold clusters. *J. Mol. Model.* **2020**, *26* (3), 58.
- (39) Sanli, S.; Altun, Y. K.; Sanli, N.; Alsancak, G. L.; Beltran, J. L. Solvent effects on pK_a values of some substituted Sulfonamides in acetonitrile-water Binary mixtures by the UV-spectroscopy method. *J. Chem. Eng. Data* **2009**, *54* (11), 3014–3021.

- (40) James, A. M.; Lord, M. P. *Macmillan's Chemical and Physical data*; Macmillan, 1992.
- (41) Bauman, S. J.; Brawley, Z. T.; Darweesh, A. A.; Herzog, J. B. Substrate oxide layer thickness optimization for a dual-width plasmonic grating for surface-enhanced Raman spectroscopy (SERS) biosensor applications. *Sensors* **2017**, *17* (7), 1530.
- (42) Cordero, E.; Korinth, F.; Stiebing, C.; Krafft, C.; Schie, I. W.; Popp, J. Evaluation of shifted excitation Raman difference spectroscopy and comparison to computational background correction methods applied to biochemical Raman spectra. *Sensors* **2017**, *17* (8), 1724.
- (43) Girmatsion, M.; Mahmud, A.; Abraha, B.; Xie, Y.; Cheng, Y.; Yu, H.; Yao, W.; Guo, Y.; Qian, H. Rapid detection of antibiotic residues in animal products using surface-enhanced Raman Spectroscopy: A review. *Food Control* **2021**, *126*, 108019.
- (44) Cialla, D.; Pollok, S.; Steinbrücker, C.; Weber, K.; Popp, J. SERS-based detection of biomolecules. *Nanophotonics* **2014**, *3* (6), 383–411.
- (45) Le Ru, E.; Etchegoin, P. *Principles of Surface-Enhanced Raman Spectroscopy: and Related Plasmonic Effects*; Elsevier, 2008.
- (46) Etchegoin, P.; Cohen, L.; Hartigan, H.; Brown, R.; Milton, M.; Gallop, J. Electromagnetic contribution to surface enhanced Raman scattering revisited. *J. Chem. Phys.* **2003**, *119* (10), 5281–5289.
- (47) Itoh, T.; Yoshida, K.; Biju, V.; Kikkawa, Y.; Ishikawa, M.; Ozaki, Y. Second enhancement in surface-enhanced resonance Raman scattering revealed by an analysis of anti-Stokes and Stokes Raman spectra. *Phys. Rev. B: Condens. Matter Mater. Phys.* **2007**, *76* (8), 085405.
- (48) Jensen, L.; Aikens, C. M.; Schatz, G. C. Electronic structure methods for studying surface-enhanced Raman scattering. *Chem. Soc. Rev.* **2008**, *37* (5), 1061–1073.
- (49) Pannico, M.; Musto, P. SERS spectroscopy for the therapeutic drug monitoring of the anticancer drug 6-Mercaptopurine: Molecular and kinetic studies. *Appl. Surf. Sci.* **2021**, *539*, 148225.
- (50) Lopez-Ramirez, M. R.; Ruano, C.; Castro, J. L.; Arenas, J. F.; Soto, J.; Otero, J. C. Surface-enhanced Raman scattering of benzoate anion adsorbed on silver nanoclusters: Evidence of the transient formation of the radical dianion. *J. Phys. Chem. C* **2010**, *114* (17), 7666–7672.
- (51) Ahmadi Peyghan, A.; Hadipour, N. L.; Bagheri, Z. Effects of Al doping and double-antisite defect on the adsorption of HCN on a BC₂N nanotube: density functional theory studies. *J. Phys. Chem. C* **2013**, *117* (5), 2427–2432.
- (52) Ahmadi, A.; Hadipour, N. L.; Kamfiroozi, M.; Bagheri, Z. Theoretical study of aluminum nitride nanotubes for chemical sensing of formaldehyde. *Sens. Actuators, B* **2012**, *161* (1), 1025–1029.
- (53) Radovic, L. R.; Bockrath, B. On the chemical nature of graphene edges: origin of stability and potential for magnetism in carbon materials. *J. Am. Chem. Soc.* **2005**, *127* (16), 5917–5927.